Sains Malaysiana 51(11)(2022): 3663-3676
http://doi.org/10.17576/jsm-2022-5111-12

Functional and Bioactive Properties of *Bupleurum chinense* DC. and *Clematis chinensis* Osbeck Mediated Biogenic Synthesized Silver Nanoparticles

(Sifat Fungsian dan Bioaktif *Bupleurum chinense* DC. dan *Clematis chinensis* Osbeck antara Nanozarah Perak Biogen Disintesis)

TER BOON SIANG[1], SINOUVASSANE DJEARAMANE[2], FANNE YEOH FERN NII[1] & ANTO CORDELIA TANISLAUS ANTONY DHANAPAL[1,*]

[1]*Department of Chemical Science, Faculty of Science, Universiti Tunku Abdul Rahman, 31900 Kampar, Perak Darul Ridzuan, Malaysia*
[2]*Centre for Biomedical and Nutrition Research Department of Allied Health Sciences, Faculty of Science, Universiti Tunku Abdul Rahman, 31900 Kampar, Perak Darul Ridzuan, Malaysia*

Received: 22 November 2021/Accepted: 7 July 2022

ABSTRACT

The synthesis of novel metallic nanoparticles (NPs) using plant materials has emerged as a cost-effective alternative to synthetic NPs and has found wide application in biomedical, cosmetic, bioremediation, and health care technology. This study aimed to synthesize and characterize the morphologies, functional groups, and crystalline structures of silver nanoparticles (AgNPs) deduced using *B. chinense* (Bc) and *C. chinensis* (Cc). The biogenic AgNPs were appraised for their antioxidant content, radical scavenging activities, antimicrobial, anti-inflammatory, and anti-diabetic activities to understand their functional and health promoting properties. The AgNPs deduced from both plants were spherical in shape with the size of 20-30 nm and possessed face centered cubic phase arrangement. The total phenolic content (TPC) was high in Cc-AgNPs (166.2100 mgGAE/g) and exhibited strong hydroxyl ($OH^{-)}$ and $ABTS^{+}$ radical scavenging activities. On the contrary, Bc-AgNPs with higher TFC (286.1438 mgQE/g) had greater nitric-oxide (NO), DPPH, Fe^{2+}scavenging and anti-albumin denaturation activities. Minimum anti-α-amylase activity disparity was observed between Cc-AgNPs (EC_{50} = 0.2903 mg/mL) and Bc-AgNPs (EC_{50} = 0.2975 mg/mL) due to various inhibition mode contributed by bioactive compounds. Besides, Bc-AgNPs showed strongest inhibition towards Gram negative bacteria while Cc-AgNPs was more effective as an antifungal agent. In conclusion, biogenic AgNPs exhibited strong functional and bioactive properties which may be attributed to the presence of bioactive compounds on the surface of AgNPs and further in-depth analysis are required to be used for various biomedical applications.

Keywords: Antioxidant activity; anti-bacterial; biogenic synthesis; *Bupleurum chinense* DC.; *Clematis chinensis* Osbeck; silver nanoparticles

ABSTRAK

Sintesis nanozarah logam (NP) novel menggunakan bahan tumbuhan telah muncul sebagai alternatif kos efektif kepada NP sintetik dan telah menemui aplikasi meluas dalam teknologi bioperubatan, kosmetik, biopemulihan dan penjagaan kesihatan. Kajian ini bertujuan untuk mensintesis dan mencirikan morfologi, kumpulan berfungsi dan struktur kristal nanozarah perak (AgNPs) yang disimpulkan menggunakan *B. chinense* (Bc) dan *C. chinensis* (Cc). AgNP biogenik dinilai untuk kandungan antioksidannya, aktiviti penghapusan radikal, aktiviti antimikrob, anti-radang dan anti-diabetes untuk memahami sifat fungsian dan kesihatannya. AgNP yang disimpulkan daripada kedua-dua tumbuhan adalah berbentuk sfera dengan saiz 20-30 nm dan mempunyai susunan fasa kubik berpusat muka. Jumlah kandungan fenolik (TPC) adalah tinggi dalam Cc-AgNPs (166.2100 mgGAE/g) dan mempamerkan aktiviti penghapusan radikal hidroksil (OH-) dan ABTS+ yang kuat. Sebaliknya, Bc-AgNPs dengan TFC yang lebih tinggi (286.1438 mgQE/g) mempunyai aktiviti denaturasi nitrik-oksida (NO), DPPH, Fe2+ dan anti-albumin yang lebih besar. Jurang aktiviti anti-α-amilase minimum diperhatikan antara Cc-AgNPs (EC50 = 0.2903 mg/mL) dan Bc-AgNPs (EC50 = 0.2975 mg/mL) disebabkan pelbagai mod perencatan yang disumbangkan oleh sebatian bioaktif. Selain itu, Bc-AgNPs menunjukkan perencatan paling kuat terhadap bakteria Gram negatif manakala Cc-AgNPs lebih berkesan sebagai agen antikulat. Kesimpulannya, AgNP biogenik mempamerkan sifat fungsian dan bioaktif yang kuat yang mungkin dikaitkan dengan kehadiran sebatian bioaktif pada permukaan AgNPs dan analisis lebih mendalam diperlukan untuk digunakan untuk pelbagai aplikasi bioperubatan.

Kata kunci: Aktiviti antioksida; anti-bakteria; *Bupleurum chinense* DC.; *Clematis chinensis* Osbeck; nanozarah perak; sintesis biogen

Introduction

Nanotechnology has been gaining traction and applied widely in the industries, pharmacology, and day-to-day life. Much research has been found pertaining to the bio-applicable nanoparticle synthesis as it has greater potential to enhance human life from various ways. AgNPs have become one of the famous nanoparticle research products due to its functional, bioactive, and biological properties that can benefit human and environment (Govindappa et al. 2018).

From reviews, chemical synthesis method applies hazardous chemical as reducing solvent and is the most common AgNPs synthesis method practiced by researchers and manufacturers. It is because it provides stable, safe, and easily controlled properties along its process. However, this method ends up with lower product yield as well as energy and fund consuming in complicated purification process (Rautela, Rani & Debnath 2019). Green synthesis method by using herbs and plants as basic material has emerged as an alternative method recently. Green synthesis of AgNPs mainly depends on phenolic, flavonoid, and other bioactive groups such as tannin, saponin or enzymes in the plants. In the process, the plant secondary metabolite will act as reducing agents to reduce silver ions (Ag^+) to silver atom or silver related molecules and stabilize the reduced Ag^0 by acting as a capping agent. The functional properties of herbs used will be enhanced by concentrated bioactive compound on surface of AgNPs (He et al. 2017).

Chinese medical herbs are widely used by mixing two or more herbs to treat diseases, boost immune system or rearrange the metabolism process of body. Thus, *Bupleurum chinense* DC. (termed as *bei chaihu* in Chinese) and *Clematis chinensis* Osbeck were chosen to synthesize AgNPs in this research, to further establish their functional and bioactive properties.

B. chinense is traditionally used to treat influenza, inflammation, malaria, menstrual disorder and hepatitis in China. This is proven to possess biofunctional features, immunomodulatory effect and hepatoprotective activity. Moreover, *B. chinense* is being used as a protective power towards liver compartment to prevent liver dysfunction or injury (Dang et al. 2019). Anti-oxidative injury aspects deal with its antioxidant activities. Anticancer properties of *B. chinense* has been proven on hepatic cancer, breast cancer, and cervical cancer by mixing *B. chinense* with other traditional Chinese medical herbs (Law, Mo & Wong 2014).

C. chinensis (termed as *wei ling xian* in mandarin) is traditionally used for anti-inflammatory, antibacterial, antitumor and as an analgesic agent. However, only antibacterial, and anti-inflammatory properties of *C. chinensis* have been studied by modern science research. Anti-inflammatory properties of solvent extracted triterpene saponin from *C. chinensis* have been successful in supressing the inflammatory related transcription factor, NF-$_K$B in rat (Peng et al. 2011). Additionally, *C. chinensis* has been reported to contain high concentration of bioactive compounds in their stem and root, which can be effectively used in production of AgNPs.

In this research, the AgNPs synthesized using *C. chinensis* and *B. chinense* root extracts were appraised for antioxidant properties, antibacterial, antifungal, anti-albumin denaturation and anti-α-amylase properties to be further explored for various applications including nutraceuticals, pharmaceuticals, and other biomedical applications.

Materials and Methods

Reagents and Instruments

B. chinense and *C. chinensis* roots were purchased from Zong Hua Chinese Medicine Centre in Melaka. $AgNO_3$, α-amylase, DPPH, ABTS and commercial AgNPs used were branded as Sigma-Aldrich (St. Louis, MO, USA). The clinical bacteria strains of *E. coli* and *S. aureus* were kindly provided by Department of Chemical Science, University Tunku Abdul Rahman. All chemicals and reagents used were of analytical grade.

The instruments used in this study are Field-emission Scanning Electron Microscope (FESEM) (JOEL USA JSM – 7610F), X-Ray Diffractometer (XRD) (Siemens D500), Fourier Transform Spectroscopy (FTIR) (Perkin-Elmer), UV-VIS Spectrophotometer (Thermo Scientific GENESYS 10), Centrifuge Machine (Sigma) and Freeze Dryer (ScanVac – coolsafe ™).

Preparation of Crude Extracts

The herbs purchased were dried at 37 °C for 7 days and grinded into powder form. Crude extracts were prepared by mixing 20 g of herb powder with 200 mL of deionized water followed by heating at 90 °C for 30 min. The plant extracts were then centrifuged at 2,500 rpm and filtered through 110 mm Smith filter paper by vacuum filtration method.

Synthesis of Silver Nanoparticles

To synthesize AgNPs, 450 mL of 10 mM $AgNO_3$ was incubated under sunlight with 50 mL of plant extract (10% w/v) for 2 h and the colour change was observed. UV-Vis spectrometry at a wavelength of 300-800 nm

was used to confirm the synthesis of AgNPs. The AgNPs colloid solution was centrifuged at 12,000 rpm for 20 min to obtain AgNPs pellet and the purified AgNPs pellet was freeze dried at -45 °C for 7 days and the AgNPs powder was stored for further use.

CHARACTERIZATION OF BIOGENIC AgNPs

UV-Visible Spectrophotometer

Influence of $AgNO_3$ concentration towards production of AgNPs was studied by treating 2-10 mM of $AgNO_3$ with plant extracts (10% w/v) in 9:1 ratio. The mixtures were subsequently exposed under sunlight for 2 h. UV-Vis spectrum of synthesized AgNPs was recorded within 300-800 nm. Wavelengths with a sharp absorption peak were identified.

XRD Analysis

In brief, AgNPs powder was mounted on the sample holder and analyzed under continuous scan from 10˚ to 80˚ at 40.0 kV, 30.00 mA at a scanning speed of 2.00 degree/ min under X-Ray Diffractometer. The wavelength of the radiation was fixed at 1.54 Å. Data was recorded every 0.02˚ intervals. Peaks obtained were compared with commercial silver database (JCPDS file no. 04 – 0783). The Scherrer equation (1) was used to analyze AgNPs' crystalline size.

$$D = \frac{K\lambda}{\beta \cos \theta} \quad (1)$$

where D represented crystallite size; K for shape factor; 0.9, λ stand for wavelength of X-Ray (1.54 Å) and β was symbolized as full width at half maximum (FHWM).

FTIR Analysis

Firstly, AgNPs powder was diluted with KBr salt in the ratio of 1:20. Then, the mixture was ground into fineness and pressed under manual hydraulic press at 4,000 psi to form an AgNP-KBr disc. The disc was then placed on the sample holder and scanned through FTIR spectrophotometer. The spectral was recorded in cm^{-1}. The functional group on the AgNP was then interpreted according to the peaks present.

FESEM Analysis

The green synthesized AgNP powder was mounted on the aluminum stub and coated with thin layer of conductive metal. Then, the coated samples were scanned through 80,000X magnification by using FESEM and the size of the AgNPs was determined using the software Image J.

ANTIOXIDANT PROPERTIES

Total Phenolic Content

In brief, 200 µL of AgNPs solution was mixed with 1 mL of Folin-Ciocalteau solution (10% v/v) and 800 µL of Na_2CO_3 (7.5% w/v). The absorbance was read at 765 nm after 30 min incubation at dark condition. Gallic acid (0-0.8 mg/mL) was used as calibration standard in this assay (Mohamed et al. 2018). The Total Polyphenol Content of AgNPs was expressed in mg Gallic acid equivalent / g dry matter (mg QE/g).

Total Flavonoid Content

Total Flavonoid Content of green synthesized AgNP was quantified by method modified from Anto Cordelia and Sharmila (2019). 200 µL of samples were incubated with 150 µL of $NaNO_3$ (5% w/v) for 6 min. Next, 150 µL of 10% $AlCl_3$ was added and incubated for 5 min. The absorbance was read at 510 nm after addition of NaOH (10% w/v). Quercetin in methanol (0-10 mg/mL) was used as standard. Total Flavonoid Content (TFC) was expressed in mg Quercetin equivalent/g dry matter (mg QE/g).

ABTS Radical Scavenging Activity

$ABTS^+$ radical scavenging ability of the green synthesized AgNPs was examined by method modified from Wong, Chai and Hoo (2012). ABTS stock solution was prepared by mixing 8 mg/mL of ABTS solution with 1.32 mg/mL of $K_2S_2O_8$ in 1:1 ratio and incubated at dark condition for 16 hours. ABTS working solution was diluted to an absorbance reading of 1.100 ± 0.005 at 734 nm by using K_3PO_4 (100 mM, pH 7.4). 100 µL of samples were incubated with 1 mL of ABTS working solution for 10 minutes at dark condition. The absorbance was read in UV-Visible spectrophotometer at 734 nm. The scavenging ability of AgNPs towards $ABTS^+$ was calculated by the formula stated below;

$$ABTS^+ \text{ Scavenging Activity (\%)} = (A_c - A_s) / A_c \times 100 \quad (2)$$

where A_c is the absorbance of negative control solution (without samples). A_s is the absorbance of solution contained samples. Ascorbic acid (0-0.1 mg/mL) was served as positive control.

DPPH Radical Scavenging Activity

Radical scavenging ability of green synthesized AgNPs towards $DPPH^+$ was carried out using methods as described by Vora, Srivastava and Modi (2017). 0.1 mM of DPPH reagent was prepared by mixing 0.0039 g of DPPH powder in 100 mL of methanol. 1 mL of sample

was incubated with 1 mL of DPPH reagent for 30 min at dark condition. The absorbance was read at 517 nm using UV-Vis spectrophotometer. The scavenging ability of AgNPs towards DPPH radical was determined by the formula stated below.

$$DPPH^{+} \text{ Scavenging activity (\%)} = (A_c - A_s) / A_c \times 100 \quad (3)$$

where A_c is the absorbance of negative control solution (without samples). A_s is absorbance of solution contained samples. Ascorbic acid (0-0.1 mg/mL) was used as positive control.

NO Radical Scavenging Activity

Griess reagent was prepared by mixing 0.1% of naphthylethylene diamine dihydrochloride and 1% of sulphanilamide in 100 mL of H_3PO_4 (2.5% v/v). About 500 µL of sample was incubated with 1 mL of 10 mM sodium nitroprusside in PBS for 3 h. The absorbance was read at 546 nm after adding 1.5 mL of Griess reagent (Panda et al. 2009). NO^{+} scavenging activity of the samples was calculated using the formula:

$$NO^{+} \text{ scavenging activity (\%)} = (A_c - A_s) / A_c \times 100 \quad (4)$$

where A_c is the absorbance of negative control solution (without samples). A_s is absorbance of solution contained samples. EDTA (0-0.5 mg/mL) served as the positive control.

OH Radical Scavenging Activity

Firstly, iron-phenanthroline (Fe-Phe) solution was prepared by dissolving both 0.099 g of 1, 10 phenanthroline and 0.077 g of $FeSO_4$ in 250 mL of sodium phosphate buffer (pH 7.4) followed by 16-h incubation at dark condition. 1 mL of sample was mixed with 2 mL of sodium phosphate buffer and 1 mL of Fe-Phe solution. 1 mL of 0.01% of H_2O_2 was then added to activate the reaction. The resultant absorbance was read at 536 nm after 60 min incubation at 37 °C (Li et al. 2008). The OH^{-} scavenging percentage of AgNPs was calculated using the given formula:

$$OH^{-} \text{ scavenging activity (\%)} = (A_s - A_n) / (A_1 - A_n) \times 100 \quad (5)$$

where A_n represented absorbance of negative control solution (without sample); A_1 is the absorbance of background control (without H_2O_2); and A_s is the absorbance of solution with samples. Gallic acid (0-0.1 mg/mL) served as the positive control.

Iron Chelating Activity Assay

Iron chelating ability of AgNPs was measured by modifying the method of Chew, Goh and Lim (2009). 400 µL of samples was made with 400 µL of 2 mM $FeCl_2$ and 800 µL of 0.25 mM ferrozine solution. The absorbance was read at 562 nm after 10 min of incubation at dark condition. The iron chelating activity of AgNPs was calculated as percentage of ferrozine-Fe^{2+} inhibited.

$$\text{Percentage of ferrozine-}Fe^{2+}\text{ complex inhibited (\%)} = (A_c - A_s) / A_c \times 100 \quad (6)$$

where A_c is the absorbance of negative control solution (without samples). A_s is absorbance of solution contained samples. EDTA (0-0.5 mg/mL) served as the positive control.

HEALTH PROMOTING PROPERTIES

Anti-albumin Denaturation Assay

Anti-albumin denaturation ability of AgNPs was examined by modifying the method of Vijayaraj, Kumar and Kumara (2018). In brief, 100 µL of sample was incubated at 37 °C for 15 min after adding 500 µL 1% BSA in PBS (pH 6.4). The mixture was then re-incubated at 70 °C for 10 min. The turbidity of the mixture was determined at 660 nm after cooled down for 20 min. The anti-inflammatory properties of AgNPs was calculated using the formula as stated below.

$$\text{Percentage of protein undenatured (\%)} = (A_c - A_s) / A_c \times 100 \quad (7)$$

where A_c is the absorbance of negative control (without samples). A_s is absorbance of solution contained samples. Acetylsalicylic acid (0-0.1 mg/mL) was used as the positive control.

Alpha-α-amylase Inhibition Assay

To begin with, DNS reagent was prepared by mixing of 2.5671 M sodium potassium tartrate and 0.026 mM of 3,5-dinitrosalicylic acid in 70 mL of 2 M NaOH followed by dilution with 900 mL of dH_2O. 200 µL of AgNPs solution was mixed with 200 µL of 1 mg/mL α-amylase in PBS (pH 6.9) and 400 µL of potato starch (0.5% w/v). After that, 100 µL of DNS reagent was added after 3 min of incubation at 37 °C. Absorbance was read at 540 nm using UV-Vis spectrophotometer after the mixture was heated to 90 °C for 15 min (Oyedemi et al. 2017). The inhibition ability was calculated as percentage of α-amylase inhibited.

Percentage of α-amylase inhibited (%) = $(A_c - A_s) / A_c \times 100$ (8)

where A_c is the absorbance of negative control (without samples). A_s is absorbance of solution contained samples. Maltose (0-0.1 mg/mL) was used as positive control.

Antibacterial Assay

Antibacterial properties of AgNPs towards Gram positive and Gram negative bacterial was done on pathogenic *E. coli* and *S. aureus* using the standard disc diffusion method. Firstly, fresh 3 h culture in LB broth matched with 0.5 McFarland standard was spread on the LB agar plates. Sterilized paper disc (6 mm) containing 200 µL of the sample was placed onto the inoculated agar plate followed by incubation overnight at 37 °C. Tetracycline was the positive control and was placed along with each plate. The zone of inhibition was then measured.

Antifungal Assay

Antifungal activity of green synthesized AgNPs was tested on pathogenic *Aspergillus niger* by disc diffusion method. A piece of 4 mm fungal culture was placed onto the middle of the plate followed by placing a piece of 6 mm sterilized disk containing 200 µL of samples onto the inoculated agar and incubated at 27 °C for 3 days. The zone of inhibition was then determined. Phenol was used as the positive control.

STATISTICAL ANALYSIS

All experiments were carried out in triplicates and reported as mean ± standard error. Statistical analyses were performed using GraphPad Prism 8. Significant levels were tested at $P < 0.05$. Each data was subjected to One-way ANOVA. Additionally, linear regression and correlation analyses were performed between TPC/TFC with bioactive function, while data from antibacterial assay was analyzed using pair parametric t-test.

RESULTS AND DISCUSSION

FORMATION OF SILVER NANOPARTICLES BY GREEN SYNTHESIS METHOD

Formation of AgNPs was primarily validated by the formation of dark brown mixture followed by peak identification at 472 nm for *C. chinensis* and 445 nm for *B. chinense*. Peak formation within 400 – 500 nm was due to excitation of surface plasmon resonance (SPR) of Ag^0 by visible light around 450 nm wavelengths, and this had served as chief indicator in AgNPs formation. Variation in product's colour and peak formation was due to differences in SPR activation and light scattering effect, which are extremely sensitive toward size, shape, dielectric environment, and distribution of AgNPs (Zhang et al. 2016) (Figures 1 & 2).

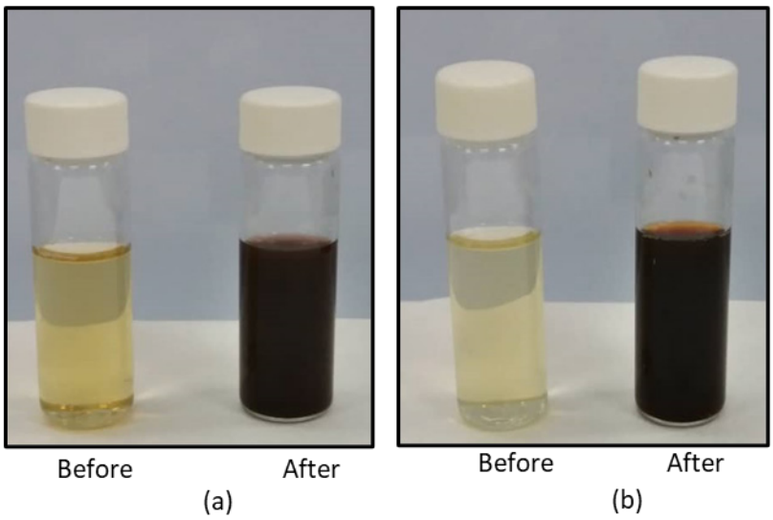

FIGURE 1. Colour Change of (a) Bc-AgNOs (left) and (b) Cc-AgNPs (right) extract indicating the formation of AgNPS

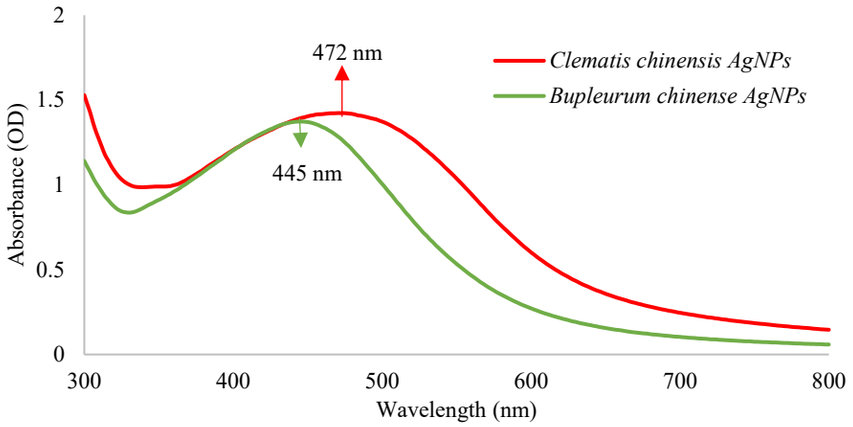

FIGURE 2. Absorption spectrum of *Bc*-AgNPs (Green) and *Cc*-AgNPs (Red)

EFFECT OF $AgNO_3$ CONCENTRATION TOWARDS THE EFFECTIVENESS OF SYNTHESIS

Effect of $AgNO_3$ precursor towards AgNPs synthesis was studied by treating constant crude extract with increasing concentration of $AgNO_3$ from 2 to 10 mM. This was the chief optimization as AgNPs will only be formed when the $AgNO_3$ reaches a suitable concentration for nucleation (He et al. 2017). Consistent increase of $AgNO_3$ concentration resulted in increased SPR intensity and significantly accelerated AgNPs yield. However, hypochromic and bathochromic shift noticed at 6 mM of $AgNO_3$ was due to size and morphology change of AgNPs. Bathochromic shifting in *Bc*-AgNPs synthesis was a result of larger particles production, increased light scattering effect and misinterpretation of actual absorbance and corresponding wavelength by the detector. However, hypochromic shift in *Cc*-AgNPs synthesis was a result of production of smaller size AgNPs which minimized the light scattering effect. Increased intensity of product solution colour with increasing $AgNO_3$ concentration was similarly observed as a continuous change in SPR (Figure 3).

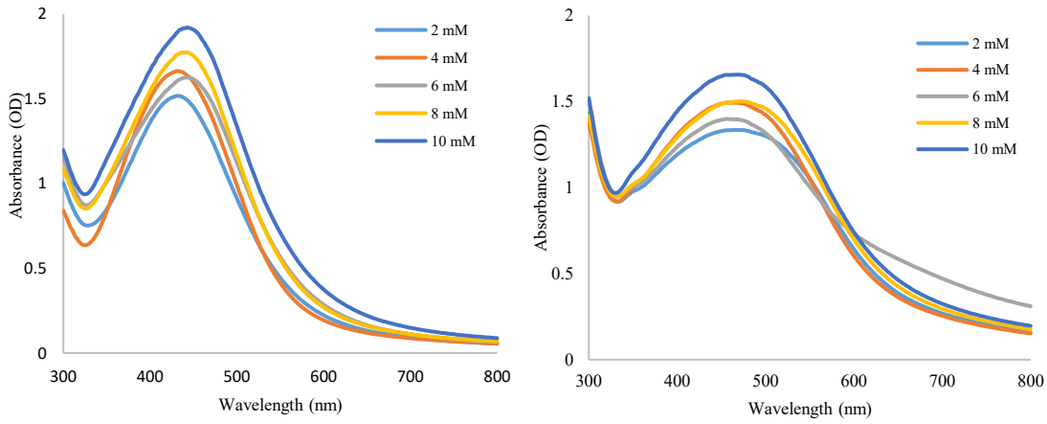

FIGURE 3. Absorption spectrum of *Bc*-AgNPs (left) and *Cc*-AgNPs (right) synthesized using different concentration of $AgNO_3$

FESEM ANALYSIS

The outer morphology and size of AgNPs was determined by FESEM. AgNPs synthesized were spherical in shape with minimum agglutination. Cooperation of green synthesis with strong sunlight radiation had produced smaller AgNPs with an average of 25.4 nm for

Bc-AgNPs and 29.1 nm for *Cc*-AgNPs which is on par with the size of commercial AgNPs (26.2 nm). Strong irradiation provided the extra energy for Ag^{+} excitation and losing electron as well as fractionate larger AgNPs into smaller fragments with extra stability (Kedi et al. 2018) (Figure 4).

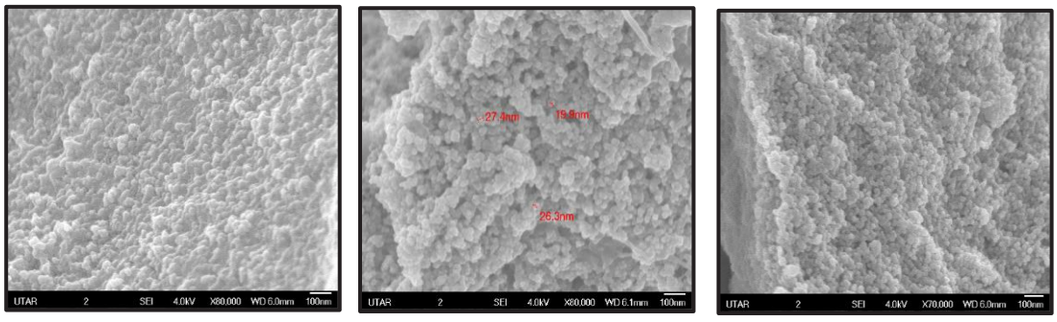

FIGURE 4. FESEM Image of *Bc*-AgNPs (left), Cc-AgNPs (middle) and c-AgNPs (right) examined under magnification of 80,000X

XRD ANALYSIS

Crystalline structure of AgNPs was confirmed by XRD pattern as shown in Figure 5. Reflection planes (111), (200), (220), and (311) indexed by diffraction peak at 38°, 44°, 64°, and 77° had been corresponding to face centered cubic structure. These parameters had showed similar characteristic with silver element. However, extra peaks at 25°, 32°, 41°, and 54° was contributed by bioactive compounds that bound on the AgNPs' surface. These bound compounds were mainly contributed by phenolic, flavonoid, protein, polysaccharide, and highly reactive compound involved in AgNPs reduction and stabilization process (Pirtarighat, Ghannadnia & Baghshah 2019) Presence of these bioactive groups were check specification.

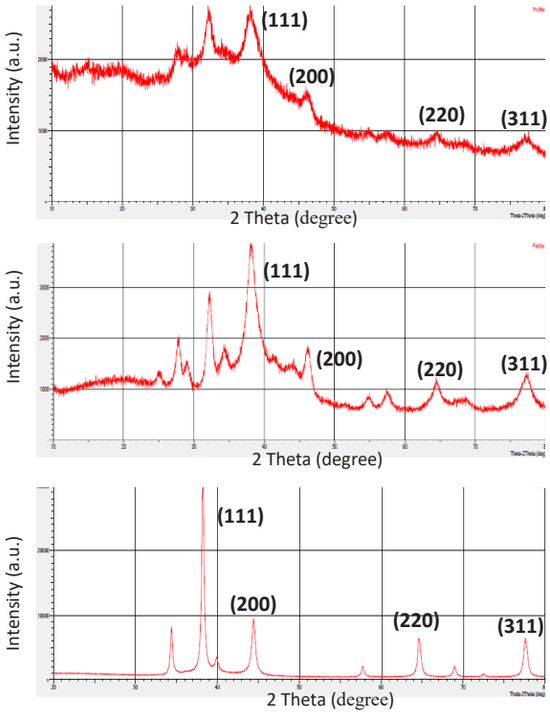

2 Theta (degree)	d-value (Å)	FWHM (degree)	Lattice constant (Å)	hkl	Crystallite size (nm)
38.3305	2.3573	1.2000	4.0830	111	7.0087
44.2600	2.0367	1.4456	4.0734	200	5.9325
64.4000	1.4422	1.3200	4.0792	220	7.1123
77.0333	1.2295	1.7733	4.0778	311	5.7257

(a) *Bc*-AgNPs

2 Theta (degree)	d-value (Å)	FWHM (degree)	Lattice constant (Å)	hkl	Crystallite size (nm)
38.2228	2.3552	1.3200	4.0793	111	6.3695
44.0600	2.0394	0.1600	4.0788	200	5.1493
64.5100	1.4444	0.4800	4.0854	220	6.9410
77.1636	1.2302	0.8400	4.0801	311	6.0466

(b) *Cc*-AgNPs

2 Theta (degree)	d-value (Å)	FWHM (degree)	Lattice constant (Å)	hkl	Crystallite size (nm)
38.1541	2.3568	0.3611	4.0821	111	23.2787
44.3291	2.0418	0.4784	4.0836	200	17.9310
64.5016	1.4435	0.3816	4.0829	220	24.6161
77.4424	1.2314	0.4360	4.0842	311	23.3541

(c) c-AgNPs

FIGURE 5. XRD Spectral of (a) *Bc*-AgNPs, (b) *Cc*-AgNPs (Middle) and (c) c-AgNPs and their respective crystallite information

FUNCTIONAL GROUP IDENTIFICATION

FTIR examination helped in determining possible interaction between bioactive compounds with *Bc*-AgNPs, *Cc*-AgNPs and c-AgNPs at a diffraction peak of 2 theta degrees. From Figures 6 and 7, vibrational band at ≈3436 cm^{-1} (OH group stretching), 1638 cm^{-1} (conjugated carbonyl and alkene compound) and 1384 cm^{-1} (aromatic benzene ring) corresponded to the phenolic and flavonoid compounds involved in the reduction of Ag^{+} to Ag^{0} (Anto Cordelia & Hng 2017). Additionally, vibration peak at ≈ 1638 cm^{-1} (α, β- unsaturated ketone compound) represented the stabilization of polysaccharide in the AgNPs capping process (Garza-Navarro et al. 2013). Besides polysaccharides, involvement of protein in the capping process was confirmed by the presence of carboxylic acid and amine (1384 cm^{-1} and 1253 cm^{-1}) and amide N-H stretching (3436 cm^{-1}, 1630 cm^{-1}). Presence of protein and polysaccharide as stabilizing agent had prevented the agglomeration of AgNPs and reduced the reactivity and toxicity of AgNPs. Coating of bioactive compounds on the surface of AgNPs was extremely dependent on surface chemical charge moieties on AgNPs with carbonyl functional group which contributed the most stability (Gatica, Cole & Velegol 2003). Absence of capping agent in c-AgNPs had exposed high toxicity and possessed unstable condition.

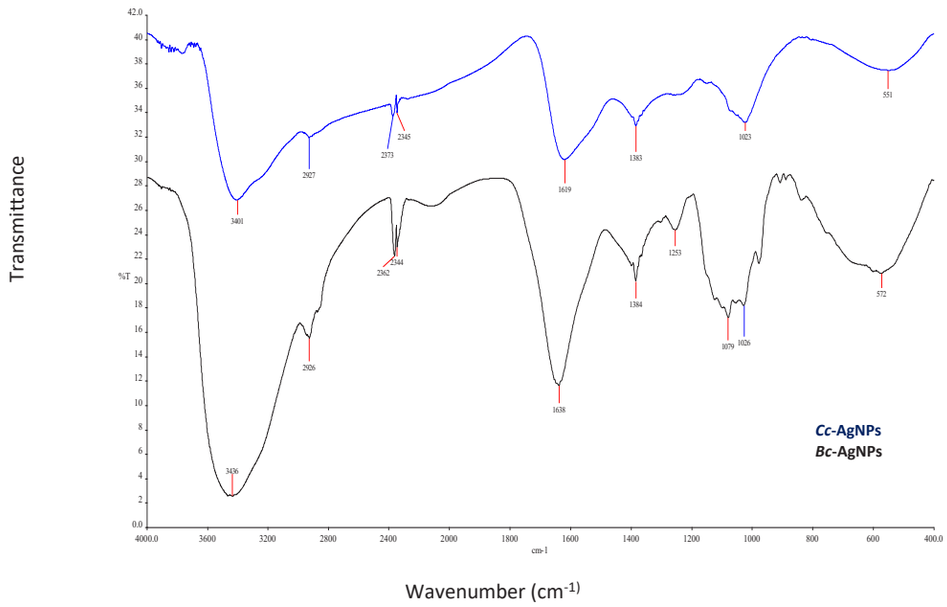

FIGURE 6. FTIR spectral of *Cc*-AgNPs (Blue) and *Bc*-AgNPs (Black)

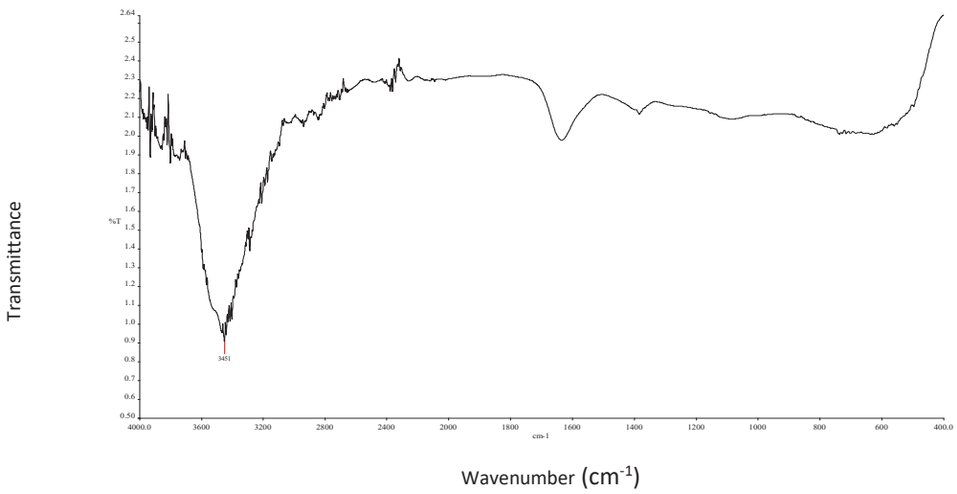

FIGURE 7. FTIR spectral of *Commercial*-AgNPs

TOTAL PHENOLIC AND FLAVONOID CONTENTS

TPC and TFC of AgNPs was quantified and expressed in mg GAE/g and mg QE/g, respectively. C-AgNPs had expressed highest TPC and TFC, while *Bc*-AgNPs expressed higher TPC than *Cc*-AgNPs, but *Cc*-AgNPs contained higher TPC than *Bc*-AgNPs. Higher TPC and TFC of AgNPs from its plant extract can be attributed to the high bioactive compounds attracted on AgNPs surface enabling to AgNPs' large surface area to volume ratio.

TABLE 1. TPC and TFC of *Bc*-AgNPs, *Cc*-AgNPs and c-AgNPs

Sample	TPC (mg GAE/g ± SE)	TFC (mg QE/g ± SE)
Bc-AgNPs	105.9411 ± 0.4310	286.1438 ± 1.7230
Cc-AgNPs	166.2100 ± 0.5156	262.1139 ± 0.5315
c-AgNPs	256.0331 ± 1.7732	331.4819 ± 0.2909

Values presented are mean of triplicate data. Each data is significant at ($p<0.005$)

ANTIOXIDANT PROPERTIES

The antioxidant properties of the AgNPs were appraised by $ABTS^+$, $DPPH^+$, NO^+, OH^- scavenging and iron chelating activity. Generally, AgNPs exhibited a concentration dependent activity towards antioxidant properties.

$DPPH^+$ is a stable bulky free radical stabilized by three bulky aromatic compounds, which accept electron from the donor. The $DPPH^+$ scavenging activity is based on the colour change of resultant solution. Higher activity was observed on *Bc*-AgNPs (EC_{50} = 0.3550 mg/mL) compared to *Cc*-AgNPs (EC_{50} = 0.4260 mg/mL) and was mainly related to limited ability of *Cc*-AgNPs in delivering the electron to $DPPH^+$ radical site. In comparison, scavenging ability of AgNPs towards $DPPH^+$ *Bc*-AgNPs' EC_{50} = 0.3550 mg/mL) was lower than NO^+ (*Bc*-AgNPs' EC_{50} = 0.2806 mg/mL) scavenging activity. This is mainly due to insufficient ability in neutralization of $DPPH^+$ compared to NO^+ (Wong et al. 2014).

For NO^+ scavenging and iron chelating activity, *Bc*-AgNPs, *Cc*-AgNPs and c-AgNPs had expressed almost similar ability, with *Bc*-AgNPs leading ahead. High cation interaction between NO^+ and Fe^{2+} with AgNPs enabled them to express higher ability than their positive control in both NO^+ and Fe^{2+} scavenging activity (Sun, Chen & Xu 2006). They scavenged almost 80% NO^+ at ≈ 0.25 mg/mL concentration and chelated 80% of Fe^{3+} at ≈ 0.5 mg/mL, compared to positive control of 0.5 mg/mL (NO^+) and 1 mg/mL (Fe^{2+}). Presence of light radiation involved in enhancement of cation interaction provided extra energy in antioxidant compounds' activation to express higher scavenging activity (Sun, Chen & Xu 2006). Nanoscale of AgNPs had provided AgNPs with efficient Fe^{2+} with ferrozine continuously delivering concentrated scavenger to Fe^{2+} and NO^+.

$ABTS^+$ and OH^- scavenging activity showed antioxidant activity of AgNPs highly related to their TPC and TFC. Lower TPC of *Bc*-AgNPs had limited its scavenging activity towards $ABTS^+$ and OH^-. This is because lower TPC had limited the H^+ availability in $ABTS^+$ and OH^- scavenging activity. Effect of TPC and TFC towards antioxidant ability was not seen notably in $DPPH^+$, NO^+ scavenging and iron chelating activity as these only depended on self-oxidation ability and radical neutralization properties of samples. However, noticeable impact in $ABTS^+$ and OH^- scavenging activity is due to this reaction that only involved H^+ from phenolic compounds (Salari et al. 2019) (Table 2).

ANTI-α-AMYLASE ACTIVITY

Anti-diabetic property of AgNPs was examined by inhibiting the carbohydrate digestive enzyme, α-amylase. *Bc*-AgNPs (EC_{50} = 0.2975 mg/mL), *Cc*-AgNPs (EC_{50} = 0.2903 mg/mL) and c-AgNPs (EC_{50} = 0.1706 mg/mL) had expressed lower inhibition capability than their positive control, maltose (EC_{50} = 0.0476 mg/mL). Higher ability of *c*-AgNPs was contributed to its higher competitive inhibition power of TPCs' H^+, which induced quinones and lactone formation at active site upon binding (Li et al. 2008). However, minimum disparity between both *Bc* and *Cc* AgNPs had been reported due to uncompetitive inhibition exhibited by others bioactive

compounds, which had provided alternative inhibition actions (Chai et al. 2016). Lower inhibition ability of green synthesized AgNPs might be due to less reactivity of bioactive compounds, stabilization process and strong bioactive compound-AgNPs binding affinity (Table 3).

TABLE 2. Antioxidant capacity of AgNPs expressed as EC_{50} values

Control/ Samples	EC_{50} values on different radical scavenging capacity in mg/mL				
	ABTS radicals	DPPH radicals	Iron chelating	NO radicals	OH radicals
Ascorbic acid	0.0535 ± 0.0029	0.0602 ± 0.0006	-	-	-
Gallic acid	-	-	-	-	0.0650 ± 0.0020
EDTA	-	-	0.5606 ± 0.0087	0.2806 ± 0.0023	-
Bc-AgNPs	0.7587 ± 0.0163	0.3550 ± 0.0095	0.3504 ± 0.0011	0.1558 ± 0.0022	1.0878 ± 0.0151
Cc-AgNPs	0.1691 ± 0.0063	0.4260 ± 0.0081	0.3514 ± 0.0020	0.1637 ± 0.0024	1.3085 ± 0.0191
c-AgNPs	0.1572 ± 0.0071	0.2724 ± 0.0252	0.6949 ± 0.0046	0.1805 ± 0.0037	0.5540 ± 0.0020

Values presented as mean of triplicate data. Each data is significant at ($p<0.005$)

TABLE 3. EC_{50} value of AgNPs and maltose in anti-α-amylase activity

Sample	EC_{50} (mg/mL
Maltose	0.0476 ± 0.0009
Bc-AgNPs	0.2975 ± 0.0004
Cc-AgNPs	1.2903 ± 0.0004
c-AgNPs	0.1706 ± 0.0003

Values are presented as mean of triplicate data. Each data is significant at ($p<0.005$)

ANTI-ALBUMIN DENATURATION ACTIVITY

c-AgNPs showed higher anti-inflammatory activity through their higher anti-albumin denaturation property. Generally, positive control, acetylsalicylic acid (EC_{50}= 0.0308 mg/mL) showed higher inhibition followed by c-AgNPs (EC_{50}= 0.0529 mg/mL), *Bc*-AgNPs (EC_{50} = 0.4570 mg/mL) and *Cc*-AgNPs (EC_{50}= 0.7266 mg/mL). High interaction between AgNPs and protein enabled AgNPs to continuously deliver concentrated bioactive reactive oxygen compounds and provide high thermal withstanding ability from thermal stable AgNPs towards protein, to subsequently provide comprehensive thermal protection on the surface of protein (Mani et al. 2016). Highly reactive status of *c*-AgNPs enabled it to expresss high thermal withstanding and reactive oxygen compounds delivery ability to enhance its anti-inflammatory function. Besides binding ability, nanoscale of AgNPs contributed as a huge bioactive compound carrier vesicle and provides sufficient interaction with the protein molecules. Furthermore, saponin and triterpene as bioactive reactive oxygen species is believed to have provided highest thermal protection towards protein in this determination (Tables 4 & 5).

TABLE 4. EC_{50} value of AgNPs and acetylsalicylic acid in anti-albumin denaturation activity

Sample	EC_{50} (mg/mL)
Acetylsalicylic acid	0.0308 ± 0.0006
Bc-AgNPs	0.4570 ± 0.0227
Cc-AgNPs	0.7266 ± 0.0080
c-AgNPs	0.0529 ± 0.0005

Values presented are mean of triplicate data. Each data is significant at ($p<0.005$)

TABLE 5. Correlation coefficient (r) of TPC/TFC with bio functional activity of *Bc*-AgNPs and *Cc*-AgNPs

Assay	Total phenolic content (TPC)		Total flavonoid content (TFC)	
	Bc-AgNPs	Cc-AgNPs	Bc-AgNPs	Cc-AgNPs
ABTS	-0.9769	-0.9993	-0.9771	-0.9983
DPPH	-0.9998	-0.9994	-0.9999	-0.9991
Iron chelating	-0.9970	-0.9961	-0.9970	-0.9986
NO	-0.9997	-0.9999	-0.9997	-0.9996
OH	-0.9994	-0.9997	-0.9997	-0.9998
AADA[a]	-0.9993	-0.9992	-0.9994	-0.9995
AAMA[b]	-0.9999	-0.9998	-0.9997	-0.9996

AADA[a] had represented Anti-albumin Denaturation Activity and AAMA[b] represented Anti-α-amylase Activity. Values presented are statistically significant ($p < 0.05$)

ANTIMICROBIAL ACTIVITY

Antimicrobial activity of AgNPs were carried out against Gram negative (*E. coli*) and Gram positive (*S. aureus*) bacteria by disk diffusion method. Results show that, AgNPs and positive control (tetracycline) displayed positive inhibition at concentration of 0.5, 1.0, and 2.0 mg/mL. AgNPs showed dose dependent inhibition activity with more effect against Gram negative bacteria, which is different from tetracycline. However, *Bc*-AgNPs was more effective towards both types of bacteria compared to *Cc*-AgNPs and c-AgNPs. Besides thin peptidoglycan cell wall, negative charges on the membrane of Gram negative bacterial had similarly shown high interaction with positively charge Ag^+ and bioactive metabolites (Tang & Zheng 2018). Adherence of toxic and reactive Ag^+ and bioactive compounds on the surface of *E. coli* had induced oxidative damage towards bacteria's cell membrane and respiratory system. Limited activity in Gram positive bacteria is possibly due to their thick peptidoglycan cell wall, which is more resistant to the oxidative disruption damage (Tang & Zheng 2018) (Figure 8 & Table 6).

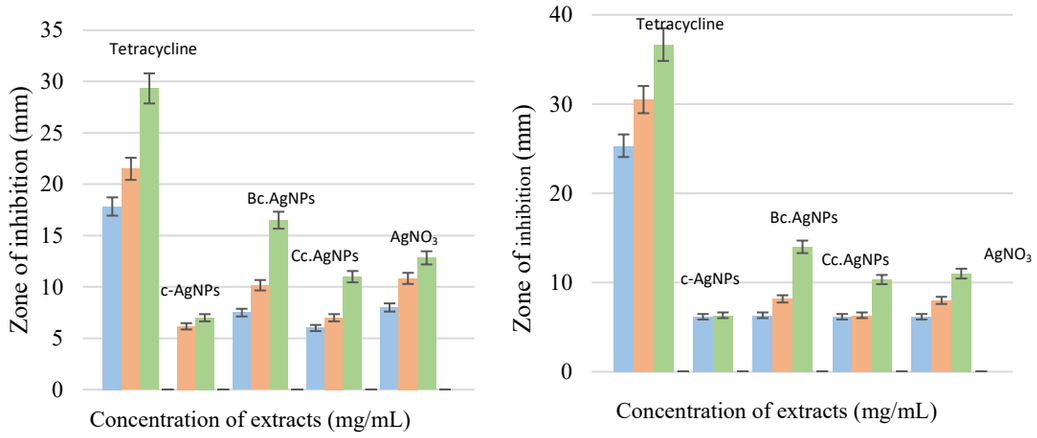

FIGURE 8. Antibacterial properties of AgNPs toward *E. coli* (a) and *S. aureus* (b)

TABLE 6. Pair parametric t-test on antimicrobial activity of AgNPs determined by *E. coli* against *S. aureus*

Sample	Pair parametric t-test		
	t-value	Mean of difference ± Standard error mean	Correlation coefficient
Tetracycline	14.990	-7.9444 ± 0.5300	0.9880*
Bc-AgNPs	4.857	1.8890 ± 0.3889	0.9981*
Cc-AgNPs	4.999	0.5556 ± 0.1111	0.9980*
c-AgNPs	1.000	0.2222 ± 0.2222	0.9963*
$AgNO_3$	6.500	2.1670 ± 0.3333	0.9719*

Values presented are statistically significant ($p < 0.05$)

ANTIFUNGAL ACTIVITY

Antifungal activity of AgNPs was conducted on pathogenic *Aspergillus niger* fungi. Similar to antimicrobial activity, the positive control, phenol showed greater inhibitory effect compared to AgNPs. Similar results were reported by Bocate et al. (2019) which showed dose dependent activity and lower inhibition ability compared to antimicrobial activity with effective concentration of 5, 7, and 10 mg/mL. *Cc*-AgNPs showed better inhibition than *Bc*-AgNPs and c-AgNPs. High inhibition of *Cc*-AgNPs was reported due to specific presence of anemonin and anemonol, which expressed high toxicity to pathological fungus (Zhou, Xie & Yan 2011). Besides, minimum size and positive charge of AgNPs may have enhanced the attraction and penetration of Ag^+ and toxic bioactive compounds to the negatively fungal membrane and induced oxidative damage towards the fungi. In contrast to antibacterial assay, AgNPs had attacked ribosome and mitochondria of fungus instead of respiratory system observed in antibacterial activity (Figure 9).

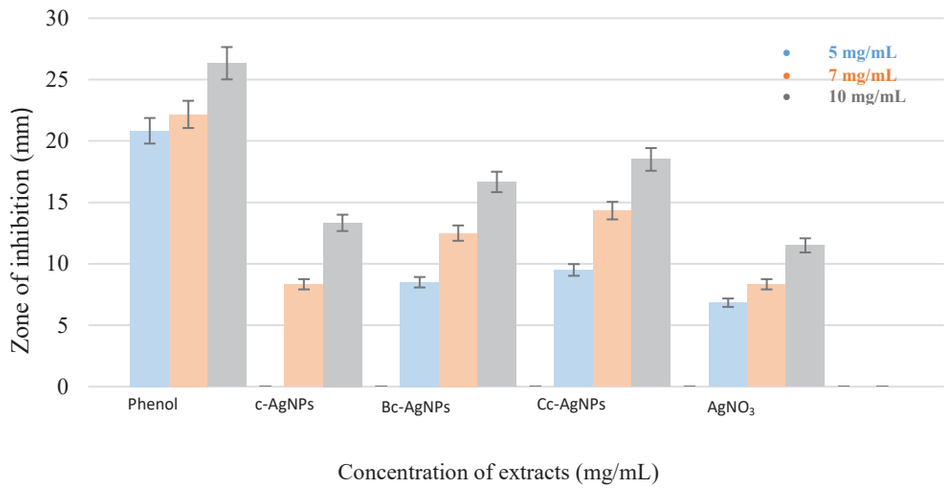

FIGURE 9. Antifungal properties of AgNPs towards *Aspergillus niger*

CONCLUSION

Aqueous extracts of *Bupleurum chinense* DC. and *Clematis chinensis* Osbeck had proven to be effective in synthesis of stable and well-defined AgNPs. Usage of medicinal herb in the synthesis of AgNPs had logical background for their use in therapeutic application. Biological synthesis method applied is eco-friendly, low cost and capable of production at room temperature. The UV-Vis spectra confirm the formation of green synthesized *Bc*-AgNPs and *Cc*-AgNPs based on surface plasmon resonance study. Bioactive compounds responsible for reducing and stabilizing of AgNPs had been confirmed by FTIR spectral. The XRD had confirmed the face centered cubic arrangement of AgNPs. FESEM results showed spherical and uniform shaped AgNPs. The AgNPs were potent in inhibiting Gram negative than Gram positive bacterial. Both *Bc*-AgNPs and *Cc*-AgNPs had showed significant in antioxidant, antifungal, anti-diabetic and anti-inflammatory activity. These baseline results have confirmed the involvement of *Bupleurum chinense* DC. and *Clematis chinensis* Osbecks' bioactive compounds in the AgNPs synthesis process and exhibited potent biological activity. Further *in-vitro* and *in-vivo* studies are required to strongly establish the health promoting behaviour of these herbs.

ACKNOWLEDGEMENTS

The authors acknowledge Universiti Tunku Abdul Rahman (UTAR), Malaysia for lab supplies and technical support. The authors do not report any conflict of interest.

REFERENCES

Anto Cordelia, T.A.D. & Hng, H.P. 2017. Investigation of green synthesized silver nanoparticles using aqueous leaf extract of *Artemisia argyi* for antioxidant and antimicrobial potentials. *International Journal of Pharmaceutical Quality Assurance* 8(4): 190-199.

Anto Cordelia, T.A.D. & Sharmila, M.D. 2019. Functional properties of novel silver nanoparticles synthesized using *Moringa oleifera*. *Acta Scientific Nutritional Health* 3(7): 190-201.

Bocate, K.P., Reis, G.F., de Souza, P.C., Oliveira Junior, A.G., Durán, N., Nakazato, G., Furlaneto, M.C., de Almeida, R.S. & Panagio, L.A. 2019. Antifungal activity of silver nanoparticles and simvastatin against toxigenic species of *Aspergillus*. *International Journal of Food Microbiology* 291: 79-86.

Chew, Y., Goh, J. & Lim, Y. 2009. Assessment of *in vitro* antioxidant capacity and polyphenolic composition of selected medicinal herb from *Leguminosae* family in Peninsular Malaysia. *Food Chemistry* 116(1): 13-18.

Chai, T., Khoo, C., Tee, C. & Wong, F. 2016. Alpha-glucosidase inhibitory and antioxidant potential of antidiabetic herb *Alternanthera sessilis*: Comparative analyses of leaf and callus solvent fractions. *Pharmacognosy Magazine* 12(48): 253-258.

Dang, Z., Li, Q., Sun, S., Wang, Y., Lin, R., Zhang, Y., Dai, J. & Zheng, N. 2019. The medicinal plant pair *Bupleurum chinense*- *Scutellaria baicalensis* – metabolomics and metallomics analysis in a model for alcoholic liver injury. *Frontiers in Pharmacology* 10: 254.

Garza-Navarro, M.A., Aguirre-Rosales, J.A., Llanas-Vázquez, E.E., Moreno-Cortez, I.E., Torres-Castro, A. & González-González, V. 2013. Totally ecofriendly synthesis of silver nanoparticles from aqueous dissolutions of polysaccharides. *International Journal of Polymer Science* 2013: 436021.

Gatica, S.M., Cole, M.W. & Velegol, D. 2005. Designing van der Waals forces between nanocolloids. *Nano Letters* 5(1): 169-173.

Govindappa, M., Hemashekhar, B., Arthikala, M., Rai, V.R. & Ramachandra, Y.L. 2018. Characterization, antibacterial, antioxidant, antidiabetic, anti-inflammatory and antityrosinase activity of green synthesized silver nanoparticles using *Calophyllum tomentosum* leaves extract. *Results in Physics* 9(1): 400-408.

He, Y., Wei, F., Ma, Z., Zhang, H., Yang, Q., Yao, B., Huang, Z., Li, J., Zeng, C. & Zhang, Q. 2017. Green synthesis of silver nanoparticles using seed extract of *Alpinia katsumadai*, and their antioxidant, cytotoxicity, and antibacterial activities. *Royal Society of Chemistry Advances* 7(63): 39842-39851.

Kedi, P.B.E., Meva, F.E., Kotsedi, L., Nguemfo, E.L., Zangueu, C.B., Ntoumba, A.A., Ahmed Mohamed, H.E., Dongmo, A.B. & Maaza, M. 2018. Eco-friendly synthesis, characterization, *in vitro* and *in vivo* anti-inflammatory activity of silver nanoparticle-mediated *Selaginella myosurus* aqueous extract. *International Journal of Nanomedicine* 13(1): 8537-8548.

Law, B.Y., Mo, J. & Wong, V.K. 2014. Autophagic effects of Chaihu (dried roots of *Bupleurum chinense* DC or *Bupleurum scorzoneraefolium* WILD. *Chinese Medicine* 9(21): 1-8.

Li, Y., Jiang, B., Zhang, T., Mu, W. & Liu, J. 2008. Antioxidant and free radical scavenging activities of chickpea protein hydrolysate (CPH). *Food Chemistry* 106(2): 444-450.

Mani, A., Vasanthi, C., Gopal, V. & Chellathai 2016. Role of phyto-stabilised silver nanoparticles in suppressing adjuvant induced arthritis in rats. *International Immunopharmacology* 41(1): 17-23.

Mohamed, Z., Ridha, O.M., Eddine, L.S. & Rebiai, A. 2018. Phenolic content, antioxidant and antibacterial activities of peel extract from *Punica granatum* L. *Research Journal of Chemistry and Environment* 22(4): 9-15.

Oyedemi, S.O., Ovedemi, B.O., Ijeh, I.I., Ohanyerem, P.E., Coopoosamy, R.M. & Aivegoro, O.A. 2017. Alpha-amylase inhibition and antioxidative capacity of some antidiabetic plants used by the traditional healers in Southeastern Nigeria. *The Scientific World Journal* 2017: 3592491.

Panda, B.N., Raj, A.B., Shrivastava, N.R. & Prathani, A.R. 2009. The evaluation of nitric oxide scavenging activity of *Acalypha indica* Linn root. *Asian Journal Research Chemistry* 2(2): 148-150.

Peng, C., Perera, P.K., Li, Y., Fang, W., Liu, L. & Li, F. 2011. Anti-inflammatory effects of *Clematis chinensis* Osbeck extract (AR-6) may be associated with NF-KB, TNF-α, and COX-2 in collagen-induced arthritis in rat. *Rheumatology International* 32(10): 3119-3125.

Pirtarighat, S., Ghannadnia, M. & Baghshah, S. 2019. Green synthesis of silver nanoparticles using the plant extract of *Salvia spinose* grown *in vitro* and their antibacterial activity. *Journal of Nanostructure in Chemistry* 9: 1-9.

Rautela, A., Rani, J. & Debnath, M. 2019. Green synthesis of silver nanoparticles from *Tectona grandis* seeds extract: Characterization and mechanism of antimicrobial action on different microorganisms. *Journal of Analytical Science and Technology* 10(5): 1-10.

Salari, S., Bahabadi, E.S., Samzadeh-Kermani, A. & Yosefzaei, F. 2019. *In-vitro* evaluation of antioxidant and antibacterial potential of green synthesized silver nanoparticles using *Prosopis farcta* fruit extract. *Iranian Journal of Pharmaceutical Research* 18(1): 430-455.

Sun, B., Chen, W. & Xu, X. 2006. Theoretical studies of the adsorption and dissociation of two NO molecules on Cu_2O (111) surface. *Acta Physico-Chimica Sinica* 22(9): 1126-1131.

Tang, S. & Zheng, J. 2018. Antibacterial activity of silver nanoparticles: Structural effects. *Advanced Healthcare Materials* 7(13): 1-10.

Vijayaraj, R., Kumar, G.D. & Kumara, N.S. 2018. *In vitro* anti-inflammatory activity of silver nanoparticles synthesized *Avicennia marina* (Forssk.) vierh.: A green synthetic approach. *International Journal of Green Pharmacy* 12(3): 528-536.

Vora, J., Srivastava, A. & Modi, H. 2017. Antibacterial and antioxidant strategies for acne treatment through plant extracts. *Informatics in Medicine Unlocked* 13(1): 128-132.

Wong, F., Chai, T. & Hoo, Y. 2012. Antioxidant and cytotoxic activities of selected medicinal herbs used in Malaysia. *Journal of Medicinal Plants Research* 6(16): 3169-3175.

Wong, F., Yong, A., Ting, E.P., Khoo, S., Ong, H. & Chai, T. 2014. Antioxidant, metal chelating, anti-glucosidase activities and phytochemical analysis of selected tropical medicinal plants. *Iranian Journal of Pharmaceutical Research* 13(4): 1407-1413.

Zhang, X., Liu, Z., Shen, W. & Gurunathan, S. 2016. Silver nanoparticles: Synthesis, characterization, properties, applications, and therapeutic approaches. *International Journal of Molecular Sciences* 17(9): 1534-1568.

Zhou, J., Xie, G. & Yan, X. 2011. *Encyclopedia of Traditional Chinese Medicines – Molecular Structures, Pharmacological Activities, Natural Sources and Applications – Vol 1: Isolated Compounds A-C.* Heidelberg: Springer Science & Business Media.

*Corresponding author; email: antoc@utar.edu.my